Journal of Stress Analysis
Vol. 6, No. 1, Spring – Summer 2021, 79-88
Bu-Ali Sina University

ORIGINAL RESEARCH PAPER

Weldability Investigation of Super-duplex Steel Hollow Pipes Welded by Gas Tungsten Arc Welding Process

Z. Ebrahimi*, A. Safaei, M. Moravej
Mechanical Engineering Department, Payame Noor University, Tehran, Iran.

Article info

Article history:
Received 12 June 2021
Received in revised form
20 August 2021
Accepted 01 September 2021

Keywords:
Welding position
Microstructure
Hardness test
Weld zone
GTAW process

Abstract

This paper investigates the weldability of super-duplex steel hollow pipes, which are welded by Gas Tungsten Arc Welding (GTAW) process, using destructive and non-destructive tests. Non-destructive inspections were performed by visual inspection and radiography, which indicate the proper quality of the performed welds. Material analysis, metallographic, tensile and hardness tests have been performed for different welding positions. The effects of the welding position on the microstructure and mechanical properties of the welded specimens were investigated. The results of the metallographic test reveal the good balance between austenite-ferrite phases in the weld zone. According to materials analysis, chromium to nickel weight percent is higher at the 12 o'clock position. The hardness test results show that the average hardness is the same in different welding positions. The presented results indicate the good weldability of the super-duplex steel pipes fabricated by the GTAW process. The weldability assessment of the GTAW super-duplex steel hollow pipes using both destructive and non-destructive tests, at different welding positions, is an innovative research.

1. Introduction

Duplex and super-duplex stainless steel alloys are widely used due to their good mechanical properties and high corrosion resistance. Most of the arc welding processes can be utilized to fabricate these steels. Welding of duplex and super-duplex steels has attracted the attention of many researchers. Labanowski [1] investigated the dissimilar connection of duplex stainless steel 2205 weldments to 316L austenitic stainless steel by duplex filler metal using an arc welding method. Mendoza et al. [2] studied the microstructure of the weld zone and the weld interface for gas tungsten arc welding of the super-duplex stainless steel with HSLA steel. Mechanical properties and corrosion resistance of 316L austenitic stainless steel to 2205 duplex steel welds have also been investigated [3]. The microstructure and mechanical properties of friction stir welded super-duplex stainless steel were investigated by Sato et al. [4]. They reported that austenite volume fraction in the weld zone is between 50 and 60% and dynamic recrystallization causes grain refinement in the stir welded zone. Tasalloti et al. [5] studied the effect of heat input on the microstructure of dissimilar welds of duplex stainless steels and ultra-high-strength steels using gas metal arc welding. The microstructure of the duplex steel joints fabricated by the flux-cored arc welding process was investigated by Hu et al. [6]. Kumar et al. [7] performed GTAW of super-duplex steel plates with 316L austenitic stainless steel. They evaluated the effects of the heat input on the resulting microstructure.

*Corresponding author: Z. Ebrahimi (Assistant Professor)
E-mail address: z.ebrahimi@pnu.ac.ir
http://dx.doi.org/10.22084/jrstan.2021.24727.1186
ISSN: 2588-2597

GTAW welding is one of the most suitable methods for joining duplex and super-duplex steel weldments and dissimilar welding. Fabrication of dissimilar aluminum-titanium lap joints has been performed utilizing the GTAW process as well [8]. Wang et al. [9] used both GTAW and shielded metal arc welding to joint dissimilar specimens of duplex stainless steel and 16MnR high strength steels. They concluded that the weldments produced by GTAW method have higher strength and corrosion resistance. The effects of the GTAW welding parameters, such as temperature and cooling rate, on the corrosion resistance of the duplex and super-duplex stainless steel weldments were determined [10]. Atif Makhdoom et al. [11] analyzed the microstructure and electrochemical behavior of the duplex 2205 steel joints welded by the GTAW method. They discussed the various phases formed in the duplex steel microstructure without heat treatment. Dokme et al. [12] used the GTAW process to conjoin Inconel 625 and AISI 316L plates with two different filler metals. They performed microstructural tests and compositional analysis to examine the quality of the weldments. The effects of thermal cycle and nitrogen content on the ductility of duplex stainless steel in the GTAW process were investigated by Varbai et al. [13]. They found that the thermal cycle had a greater effect on the amount of austenite to ferrite in the microstructure of the alloy produced by the GTAW process. Pickle et al. investigated the root pass microstructure of super-duplex steels multi-pass joints welded by the GTAW process [14]. They showed that the austenite-ferrite volume fraction is balanced in multi-pass tungsten arc welding. In a recent study, the effect of heat treatment on the structure and mechanical properties of super-duplex steel joints produced by the GTAW was estimated [15]. Khan et al. [16] investigated the reformed austenite in the microstructure of joints between super-duplex stainless steel joints and pipeline steel welded by GTAW process.

Despite extensive research in the welding of the duplex steels, the weldability assessment of the super-duplex pipes fabricated by the GTAW process has not been reported in the literature. In all of the mentioned literature, the steel specimens were plates or lap joints. Welding of the steel pipes and the effects of welding position on their mechanical properties has been done only for low-carbon steels [17]. Therefore, this paper aims to assess the weldability of the super-duplex steel hollow pipes welded by the GTAW process. The microstructure and mechanical properties of the GTAW super-duplex steel pipes are determined using destructive tests (DTs) and non-destructive tests (NDTs) in this research. According to the best of the authors' knowledge, the weldability investigation of the super-duplex steel hollow pipes, using both destructive and non-destructive tests, is a new and innovative research.

2. Materials and Methods

The chemical composition of the UNS 32750 super-duplex steel and the ER2594 filler metal are given in Table 1. The super-duplex ER2594 filler metal has been successfully utilized in the GTAW of the duplex and super-duplex steels [18]. The material analysis procedure, which is used for determination of the chemical compositions, is described in section 3.2.1.

Table 1
Chemical composition of the filler metal and the super-duplex steel (weight percent).

Elements	UNS 32750	ER2594
C	0.012	0.010
Mn	0.75	0.60
Si	0.26	0.50
P	0.022	0.02
S	0.001	<0.01
Cr	24.79	25.1
Ni	6.94	9.3
Mo	3.84	3.9
N	0.28	0.26
Cu	0.25	0.1
W	0	0.1

The pipe specimen at different welding positions for the GTAW process is shown in Fig. 1. The pipe is fixed in horizontal direction and the welding groove is placed vertically. The welding process is performed in three passes from the bottom to up direction. The specimen is pre-heated to prevent distortion and the welding groove is in the middle of the pipe. The welding details are according to the WPS standard. The welding current is 85A and with a voltage of 10V. The pipe is fixed at 45° for orbital welding. After cleaning and preparing the specimens, the welding process was performed at four positions, i.e., 3, 6, 9, and 12 o'clock as shown in Fig. 1.

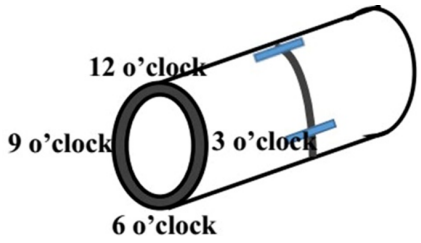

Fig. 1. The hollow pipe specimen placed at the 3, 6, 9, and 12 o'clock positions for the GTAW process.

The non-destructive tests performed in this study include the visual inspections and radiographic tests. Visual inspection is usually applied to identify the surface defects. The device and equipment used for the visual inspection of the GTAW pipe weldments are thermometers, temperature-sensitive colored pencils, and the ferrite phase measuring instruments. Inspection

reports should be concise and at the same time complete enough to be clear to anyone unfamiliar with the product being inspected. The results of this inspection are reported in the next section. The radiographic inspection of the hollow pipes is one of the most widely used non-destructive testing (NDT) methods to detect internal defects in these structures. Surface defects can also be detected by radiography with appropriate orientation; this method is also used to find compositional changes in materials, thickness measurements, and to locate the damaged specimens, which are placed inside the devices and are hidden from the visual inspection. NDTs are performed according to the requirements and methods specified in the ASME Sex V.

Destructive test specimens are prepared according to the WPS. The number and size of the test specimens are prepared according to the QW-450 and QW-460 IX standards. The destructive tests, considered in this study, are the tensile test, the hardness test to evaluate the effective penetration of the welded joints, the metallographic test and the material analysis in the Aeat-Affected Zone (HAZ) and the Weld Zone (WZ).

Hardness of the weldments is measured using the Vickers hardness tester in this study. Both microscopic and macroscopic investigations are performed in the metallographic tests. For this purpose, each sample was rinsed and macro etched to identify the WZ, HAZ, and the Base Metal (BM). The microstructure investigations are performed with optical microscope with 200X and 500X magnifications. The microstructure of the BM, HAZ, and the WZ is investigated for different welding positions, i.e., 3, 6, 9, and 12 o'clock positions.

3. Results and Discussion

In this section, the results of the destructive and non-destructive tests, which are performed on the GTAW super-duplex steel hollow pipes, are presented.

3.1. NDTs Results

The results of NDTs, which include visual and radiographic inspections, are reported in this section. First, the visual inspection is considered. The results of the visual inspection of the welded pipes reveal that the weld is free of cracks and the surface of the weld is in good contact with the outer wall of the pipe. The weld root is inspected and is found to be free of the cracks. No incomplete melting with inadequate penetration is observed. Moreover, root pass concavity, with an allowable amount of 1.6mm, and the width of the weld melt, with a maximum value of 3.2mm, are examined and appropriate results are obtained. Consequently, the results of the visual inspection indicate the excellent quality of the GTAW super-duplex steel pipe weldments.

Fig. 2. Radiographic image of a super-duplex steel pipe welding sample.

The next non-destructive test in this study is the radiographic inspection. The interpretation of the radiographic inspection was performed in three stages, i.e., detection, interpretation, and evaluation. Fig. 2. shows the image obtained from the radiographic inspection. As depicted in Fig. 2., the fusion of the base metal is adequate and the weld zone and the base metal are completely bonded together. The radiograph does not show any dark or irregular areas on the weld and no slag inclusions are observed in the radiograph of the weld. The incomplete penetration, which can be presented in the form of dark spots or smooth lines, is not observed. Incomplete fusion usually appears in the form of a dashed line or oriented lines in the direction of the weld interface. The filler weld metal and the base metal are appropriately combined and no dashed or oriented lines are observed on the radiograph.

3.2. DTs Results

The results of the destructive tests, i.e. material analysis, tensile, hardness, and metallographic tests, are presented in this section.

3.2.1. Material Analysis

The chemical composition of duplex stainless steels plays an important role in their final properties. Therefore, it is necessary to determine the chemical composition of the welding samples. The material analysis test was performed by diffusion spectrometry at room temperature of 25°C and ambient humidity of 30%. Table 2 shows the chemical composition of the weld root and the weld surface at the 6 and 12 o'clock positions. The weight percent of the chromium-nickel at the 12 o'clock position at the weld surface has the maximum value. The nickel weight percent at different positions in the weld zone is approximately the same, but is higher than that of the base metal. The silicon weight percent at the 12 o'clock position of the WZ is slightly higher than of other welding positions. The results of the material analysis, according to the appropriate chromium-nickel volume fraction, indicate the good quality and strength of the fabricated weld for all welding positions. Fig. 3 shows the specimens after material analysis for 6 and 12 o'clock welding positions.

Table 2
Chemical composition of the weld root and the weld surface at the 6 and 12 o'clock (weight percent).

%	6 o'clock weld root	6 o'clock weld surf.	12 o'clockWeld Root	12 o'clock weld surf.
C	0.01	0.02	0.01	0.01
Si	0.46	0.46	0.52	0.50
Mn	0.56	0.54	0.57	0.57
P	0.030	0.033	0.035	0.035
S	0.015	0.015	0.015	0.015
Cr	25.2	24.3	25.6	26.7
Mo	3.8	3.8	3.6	3.6
Ni	8.7	8.5	8.7	8.6
Al	0.013	0.018	0.014	0.014
Co	0.11	0.13	0.10	0.07
Cu	0.12	0.11	0.11	0.10
Nb	0.05	0.05	0.06	0.06
Ti	0.01	0.003	0.002	0.002
V	0.06	0.05	0.06	0.06
W	0.06	0.06	0.07	0.06
Fe	Base	Base	Base	Base

Fig. 3. The specimens after material analysis at the 6 and 12 o'clock welding positions.

3.2.2. Tensile Test

The tensile test of the super-duplex pipe specimens welded by the GTAW is performed at 25°C and 40% humidity according to the ASME SEX IX standard. The results of the tensile test are presented in Table 3. Five samples are examined for each welding position during the tensile testing, and the average values of the tensile test results are reported in Table 3. The ultimate strength and the yield strength have higher values at the 6 o'clock welding position. However, the tensile strength has an acceptable value for all welding positions.

Fig. 4 shows the specimens which are prepared for the tensile tests at the 6 and 12 o'clock welding positions before testing. The damaged specimens after the tensile tests are illustrated in Fig. 5. For the specimen at the 6 o'clock position, the failure occurred at the weld zone. For the 12 o'clock position, the failure occurred in the base metal of the welded specimen. The fact that the failure did not occur at the weld zone of the 12 o'clock sample, could be attributed to the higher chromium content at the WZ for this position. According to the materials analysis results in Table 2, the chromium volume fraction is relatively high at the WZ for the 12 o'clock position.

Table 3
Tensile test results at the 6 and 12 o'clock welding positions.

	6 o'clock	12 o'clock
Dimensions (mm)	19.07 × 3.11	19.08 × 3.19
Cross section area (mm^2)	59.30	60.87
Yield strength (MPa)	788	783
Ultimate strength (MPa)	892	883
Fracture position	WZ	BM

Fig. 4. Tensile test specimens before testing.

3.2.3. Hardness Test

Harness tests across the welded specimens are performed using a Vickers micro hardness tester with a load of 10kg. The location of the points, where the hardness was measured, is shown in Fig. 6. Two lines, which the hardness was taken along them, are illus-

trated in Fig. 7. The points numbered 1 to 23 are along the upper line in the weld and the line from 24^{th} to 40^{th} points is placed at the lower part of the welded specimen. The hardness tests are performed for two welding positions, i.e., 6 and 12 o'clock. All the tests are performed at room temperature and a humidity of 40%.

Fig. 5. Tensile test specimens after testing.

Fig. 6. The specimen examined in the hardness test.

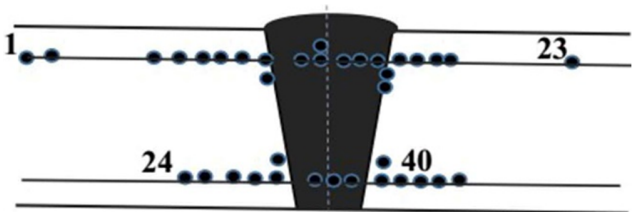

Fig. 7. The sample points for the hardness test.

The hardness test results are presented in Table 4. The average values of the hardness are almost the same in the BM and the HAZ. However, in the HAZ at points 8 and 9, which are closer to the weld zone, the hardness is slightly higher (about 2%). In the weld zone, points 10 to 16, the hardness decreases. In the lower line marked of the weld zone, i.e., points 31 to 34, a decrease in hardness of about 7% is observed, as well.

The hardness profile across the weld, and along the lines marked in Fig. 7, are presented in Fig. 8 and Fig. 9, for the 6 o'clock and 12 o'clock positions, respectively. Fig. 8 shows the hardness profile for the 6 o'clock position. The reduction in stiffness in the WZ region is clearly shown in this figure. Fig. 9 similarly shows the hardness profile for the 12 o'clock position, in which the stiffness reduction in the WZ has a similar trend to that of Fig. 8. Therefore, the welding position does not have a significant effect on the welding hardness. The average hardness values are adequate in all welding positions; this reveals the high quality of the super-duplex steel pipes specimens welded by the GTAW process.

Table 4
Hardness test results at the 6 and 12 o'clock welding positions.

Point		Hardness (HV) 6 o'clock	Hardness (HV) 12 o'clock
1	BM	319	297
2		297	299
3		299	294
4		297	292
5	HAZ	294	294
6		294	297
7		297	294
8		302	302
9		304	306
10	WZ	276	276
11		272	274
12		270	276
13		272	272
14		272	274
15		274	276
16		276	274
17	HAZ	297	299
18		302	297
19		299	294
20	BM	297	294
21		294	297
22		294	294
23		297	297
24	BM	292	294
25		294	292
26		297	297
27	HAZ	297	294
28		294	297
29		299	299
30		302	302
31	WZ	276	279
32		272	276
33		274	274
34		272	276
35	HAZ	297	297
36		294	299
37		297	297
38	BM	299	299
39		302	294
40		292	302

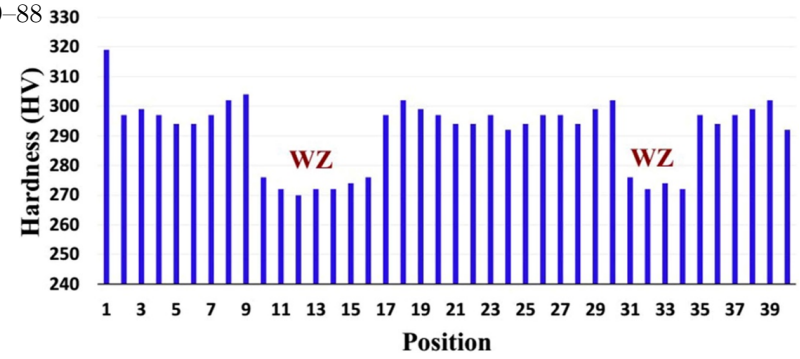

Fig. 8. The hardness profile at the 6 o'clock welding position.

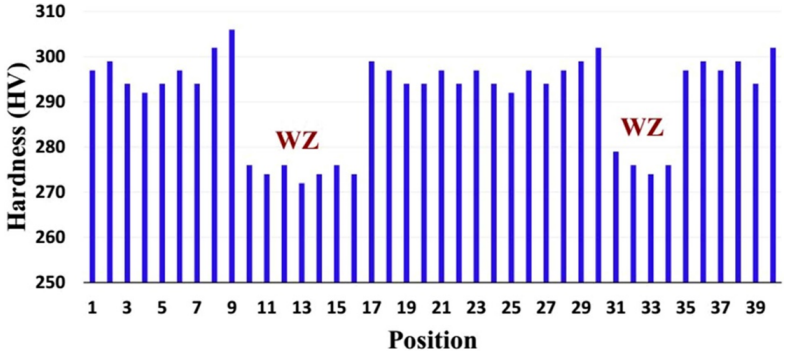

Fig. 9. The hardness profile at the 12 o'clock welding position.

3.3. Metallographic Tests

In order to study the microstructure of the base metal, the welding zone, and the heat-affected zone, the metallographic test is performed. As mentioned before, these experiments are carried out in two parts, i.e., macroscopic and microscopic investigations.

First, the results of the macroscopic tests are reported. The samples for the macroscopic study are rinsed with suitable chemical solutions and are macro etched to identify the different zones, i.e., BM, HAZ, and WZ. The results of the macroscopic tests are illustrated in Figs. 10 and 11. The sample after mounting is shown in Fig. 12. According to Figs. 10 and 11, the weld has an acceptable profile and convexity. The fusion of the weld root is adequate. The weld penetration in the base metal and different welding layers is suitable. The weld penetration at 25X magnification is crack-free. The BM and HAZ are also free of cracks. The weldments are free of cavities, slag impurities and other welding defects.

Next, the microscopic test results are reported. The microstructure study is performed after the hot mounting of the samples. The microscopic structure of the 6 o'clock welding position, which is obtained by the optical microscopy with the 200X magnification, is shown in Fig. 13. Fig. 13a shows the duplex structure in the BM. The HAZ and the WZ microstructures are shown in Figs. 13b and 13c, respectively. Fig. 14 shows the duplex structure at the 12 o'clock welding position, similarly.

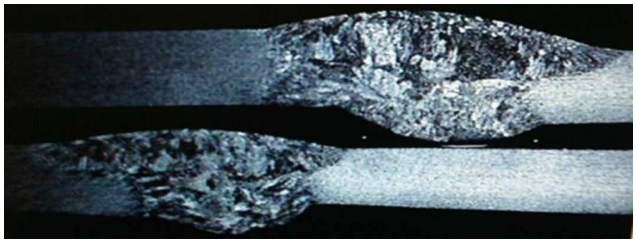

Fig. 10. The macroscopic image of a weld at the 6 o'clock welding position.

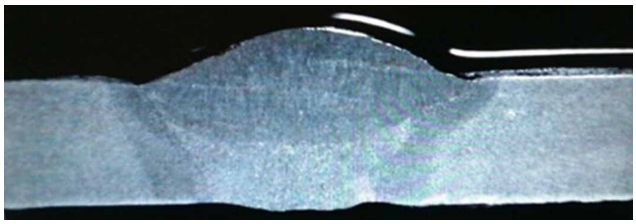

Fig. 11. The macroscopic image of a weld at the 12 o'clock welding position.

Fig. 12. The sample mounting.

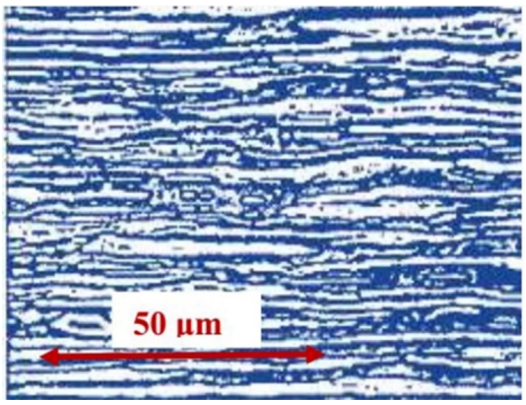

(a)

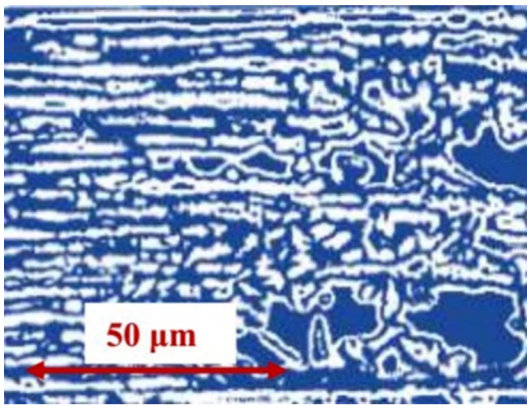

(b)

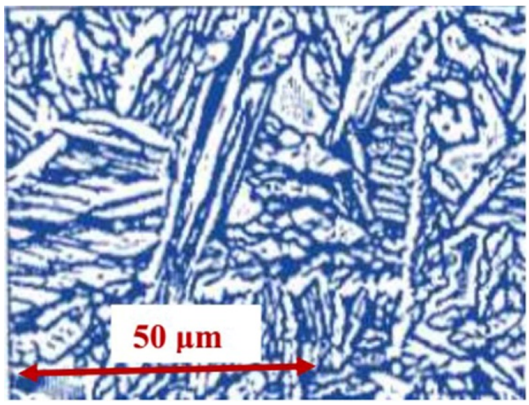

(c)

Fig. 13. Duplex structure at the 6 o'clock position; a) BM, b) HAZ, c) WZ.

Examination of the microstructures obtained by optical microscopy shows that the microscopic structure of the base metal includes a strip duplex structure containing the austenite phase (light phase) in the ferrite field (dark phase). The microscopic structure in the HAZ region near the weld of the coarse-grained duplex structure consists of the austenite phase in the ferrite field, which contains secondary austenite needle particles in the ferrite field and grain boundaries. In the weld zone, the duplex structure consists of the austenite phase and ferrite phase with secondary austenite needle-like particles in the ferrite field.

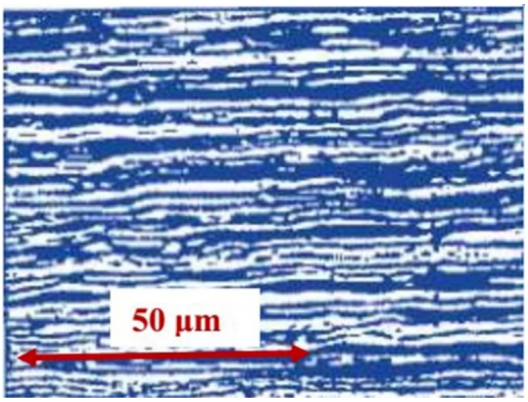

(a)

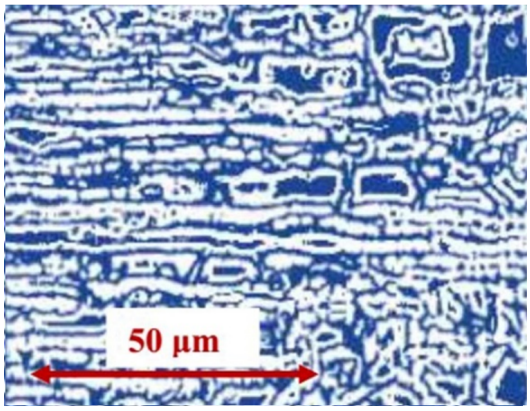

(b)

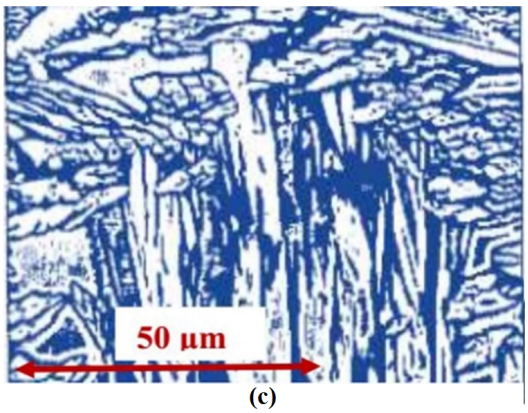

(c)

Fig. 14. Duplex structure at the 12 o'clock position; a) BM, b) HAZ, c) WZ.

Figs. 15 to 18 show the optical microscope images at the 500X magnification, after etching with glycerol at 3, 6, 9, and 12 o'clock welding positions. For the 3 o'clock position, the dual-phase austenite-ferrite structure of the HAZ is shown in Fig. 15a and of the WZ in Fig. 15b. Using these images, it is possible to determine the volume fraction of austenite-ferrite phase at different welding positions.

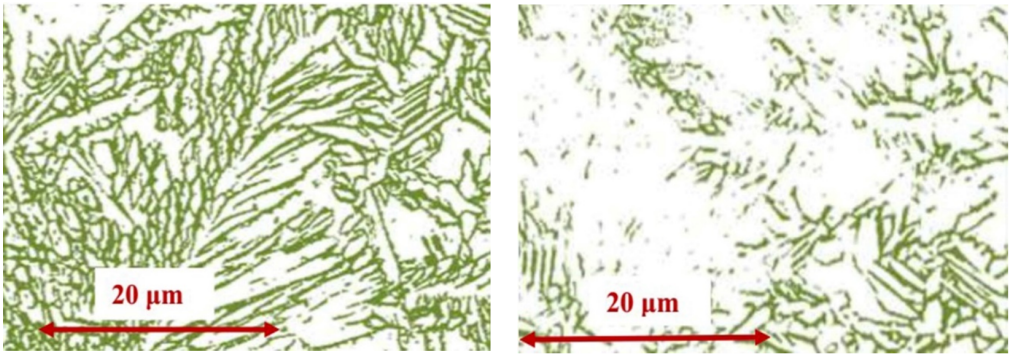

Fig. 15. Two-phase structure of austenite-ferrite at the 3 o'clock position; a) HAZ, b) WZ.

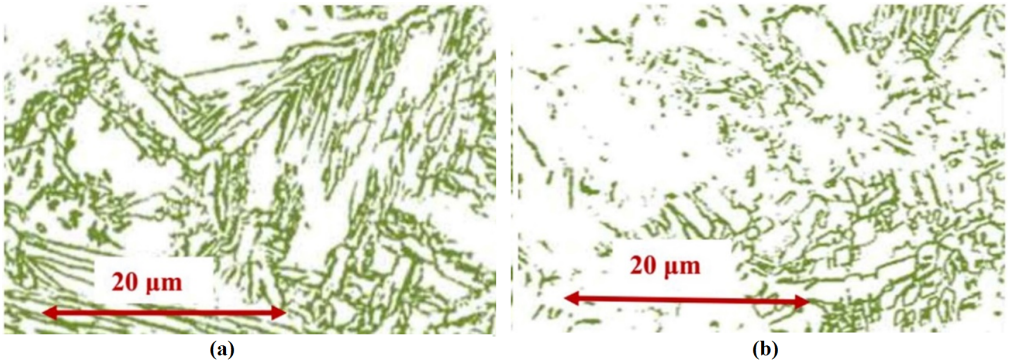

Fig. 16. Two-phase structure of austenite-ferrite at the 6 o'clock position; a) HAZ, b) WZ.

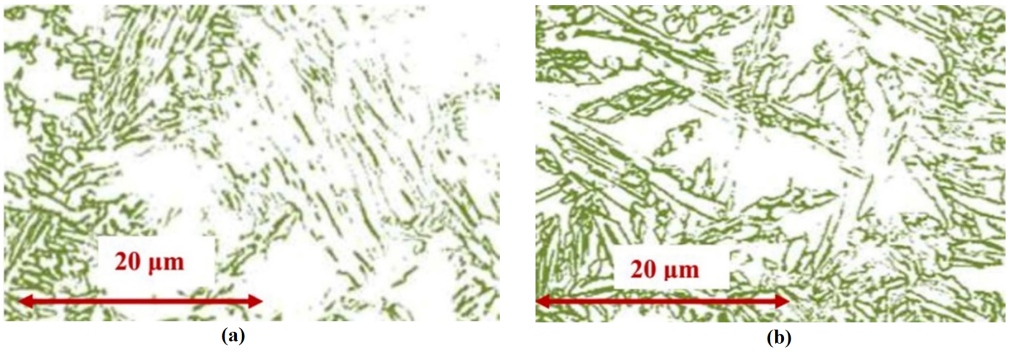

Fig. 17. Two-phase structure of austenite-ferrite at the 9 o'clock position; a) HAZ, b) WZ.

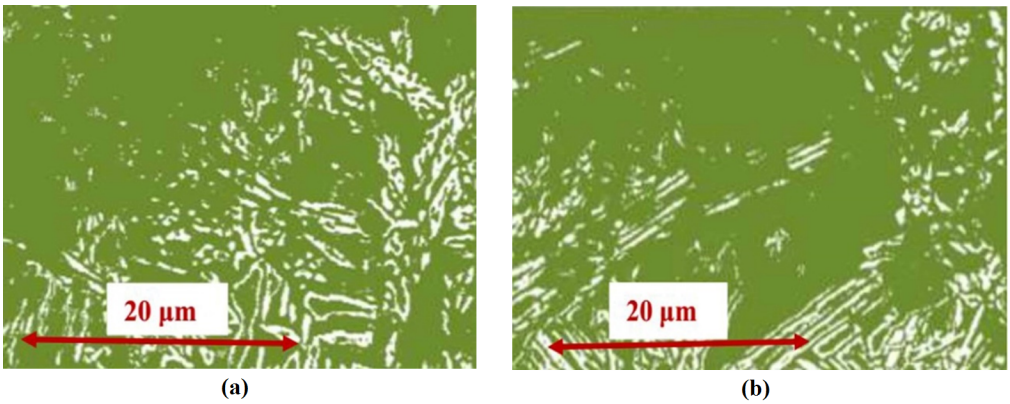

Fig. 18. Two-phase structure of austenite ferrite at the 12 o'clock position; a) HAZ, b) WZ.

Table 5
Volume fraction of the ferrite phase for different welding positions (weight percent).

Point	3 o'clock	6 o'clock	9 o'clock	12 o'clock
1	47.5	40.0	47.5	47.5
2	40.0	42.5	42.5	42.5
3	45.0	42.5	50.0	45.0
4	45.0	46.6	46.7	48.3
5	48.3	45.0	44.1	46.6
6	47.5	45.8	45.0	43.3
7	47.5	47.5	50.0	47.5
8	50.0	45.0	47.5	45.0
9	45.0	40.0	47.5	42.5

The austenite and ferrite phase volume fractions are evaluated for different welding positions in the WZ and the HAZ. The volume fractions of the ferrite phase for different welding positions are presented in Table 5. Points 1 to 4 correspond to the WZ and the points 5 to 9 correspond to the HAZ. Only at one point, for the 3 o'clock and 6 o'clock positions, in the weld zone, the volume fraction of the austenite phase (light phase) is 60% and the volume fraction of the ferrite phase (dark phase) is 40%. In other points, the ferrite volume fraction is balanced with the austenite phase with an average value of 50%. The good balance between the austenite-ferrite phases in the super-duplex steels GTAW pipe welds indicates the good quality of the super-duplex steel pipe weldments.

4. Conclusions

In this study, the weldability of super-duplex steel hollow pipe specimens, which were welded by the GTAW process, was investigated using the destructive and non-destructive tests. Based on the presented results, the main conclusions of this research can be drawn as follows:

1. Observation of complete melting, suitable root pass concavity, and no cracks on the weldments during the visual inspection reveal the good quality of the performed welds. Adequate fusion of the base metal and its appropriate bonding to the weld zone and observation of no slag inclusions in the radiographic inspection, represent an excellent quality of the super-duplex steel pipe weldments fabricated by the GTAW process.

2. The hardness test results show that the average hardness is the same in different welding positions. The hardness of the weld zone was less than the hardness of the heat-affected zone for all welding positions. However, the average value of the weld hardness was appropriate for all welding positions.

3. As a result of the metallographic tests, a good balance between ferrite-austenite phases was obtained for all welding positions. The appropriate equilibrium between austenite-ferrite phases, which reduces the formation of the coarse ferrite grains in the heat-affected zone, reveals the good weldeability of the super-duplex steel pipe weldments.

4. According to material analysis, the volume fraction of chromium to nickel is higher at the 12 o'clock position. Therefore, the failure did not occur at the weld zone of the 12 o'clock sample during the tensile test.

5. The tensile strength had an acceptable value for all welding positions; however, the ultimate and the yield strengths were higher at the 6 o'clock welding position.

6. The good equilibrium between austenite/ferrite phases, the appropriate hardness and the tensile strength, the high volume fraction of chromium to nickel phases for all welding positions, and the results of the non-destructive tests indicate the good weldability of super-duplex steel pipes fabricated by the GTAW process in this study.

Acknowledgements

This research did not receive any specific grant from funding agencies in the public, commercial, or not-for-profit sectors.

References

[1] J. Labanowski, Stress corrosion cracking susceptibility of dissimilar stainless steels welded joints, J. Achiev. Mater. Manuf., 20(1-2) (2007) 255-258.

[2] B.I. Mendoza, Z.C. Maldonado, H.A. Albiter, P.E. Robles, Dissimilar welding of superduplex stainless steel / HSLA steel for offshore application joined by GTAW, Sci. Res. J., 2(7) (2010) 520-528.

[3] J. Labanowski, Mechanical properties and corrosion resistance of dissimilar stainless steel welds, Arch. Mater. Sci. Eng., 28(1) (2007) 27-33.

[4] Y.S. Sato, T.W. Nelson, C.J. Sterling, R.J. Steel, C.O. Petterson, Microstructure and mechanical properties of friction stir welded SAF 2507 super duplex stainless steel, Mater. Sci. Eng. A, 397(1-2) (2005) 376-384.

[5] H. Tasalloti, P. Kah, J. Martikainen, Effect of heat input on dissimilar welds of ultra high strength steel and duplex stainless steel: Microstructural and compositional analysis, Mater. Charact., 123 (2017) 29-41.

[6] Y. Hu, Y. Shi, K. Sun, X. Shen, Zh. Wang, Microstructure and mechanical properties of underwater hyperbaric FCA-welded duplex stainless steel joints, J. Mater. Process. Tech., 261 (2018) 31-38.

[7] N. Kumar, A. Kumar, A. Gupta, A.D. Gaikwad, R.K. Khatirkar, Gas tungsten arc welding of 316L austenitic stainless steel with UNS S32205 duplex stainless steel, Trans. Indian Inst. Met., 71 (2018) 361-372.

[8] A. Akhtar, H. Dong, Y. Xia, P. Li, Lap joining 5052 aluminum alloy to Ti6Al4V titanium alloy by GTAW process with AlSi12 filler wire, China Weld., 29 (3) (2020) 1-8.

[9] S. Wang, Q. Ma, Y. Li, Characterization of microstructure, mechanical properties and corrosion resistance of dissimilar welded joint between 2205 duplex stainless steel and 16MnR, Mater. Des., 32(2) (2011) 831-837.

[10] P. Paulraj, R. Garg, Effect of welding parameters on pitting behavior of GTAW of DSS and super DSS weldments, Eng. Sci. Technol. Int. J., 19(2) (2016) 1076-1083.

[11] M. Atif Makhdoom, A. Ahmad, M. Kamran, K. Abid, W. Haider, Microstructural and electrochemical behavior of 2205 duplex stainless steel weldments, Surf. Interfaces, 9 (2017) 189-195.

[12] F. Dokme, M.K. Kulekci, U. Esme, Microstructural and mechanical characterization of dissimilar metal welding of Inconel 625 and AISI 316L. Metals., 8(10) (2018) 797.

[13] B. Varbai, Y. Adonyi, R. Baumer, T. Pickle, J. Dobránszky, K. Májlinger, Weldability of duplex stainless steels-thermal cycle and nitrogen effects, Weld. J., 98 (2019) 78-87.

[14] T. Pickle, N. Henry, P. Morriss, L. Tennis, D. Wagner, R.E. Baumer, Root pass microstructure in super duplex stainless steel multipass welds, Weld. J., 98 (2019) 123-134.

[15] K. Qi, G. Wang, Y. Jin, J. Gu, Zh. Zhang, Y. Tao, Effect of heat treatment on structure and properties of GTAW and laser beam welded super-duplex stainless steel joints, Int. J. Mod. Phys. B, 34(01n03) (2020) 2040061.

[16] W.N. Khan, S. Mahajan, R. Chhibber, Investigations on reformed austenite in the microstructure of dissimilar super duplex/pipeline steel weld, Mater. Lett., 285 (2021) 129109.

[17] D.W. Figueirôa, I.O. Pigozzo, R.H. Gonçalves e Silva, T.F. Santos, S.L. Urtiga Filho, Influence of welding position and parameters in orbital tig welding applied to low-carbon steel pipes, Weld. Int., 31(8) (2017) 583-590.

[18] A. Kellai, A. Lounis, S. Kahla, B. Idir, Effect of root pass filler metal on microstructure and mechanical properties in the multi-pass welding of duplex stainless steels. Int. J. Adv. Manuf. Technol., 95 (2018) 3215-3225.